Journal of Power Sources 191 (2009) 139–143

Contents lists available at ScienceDirect

Journal of Power Sources

journal homepage: www.elsevier.com/locate/jpowsour

Short communication

Numerical simulation of electrolyte particles trajectory to investigate battery cover design characteristics

Vahid Esfahanian [a,*], Hossein Mahmoodi Darian [a], Hamed Babazadeh [a], Maziar Aghvami [a], Reza Pasandeh [a], Farschad Torabi [a], Goodarz Ahmadi [b]

[a] Vehicle, Fuel and Environment Research Institute, Faculty of Mechanical Engineering, University College of Engineering, University of Tehran, Tehran 11365-4563, Iran
[b] Department of Mechanical and Aeronautical Engineering, Clarkson University, Potsdam, NY 13699-5725, United States

ARTICLE INFO

Article history:
Received 31 July 2008
Received in revised form
16 September 2008
Accepted 17 September 2008
Available online 10 October 2008

Keywords:
Battery lid
Particle trajectory
Maintenance-free
Numerical simulation

ABSTRACT

In this research, a numerical simulation has been conducted to investigate one of the important factors for the efficient design of a maintenance-free (MF) lead-acid battery lid. Baffles and splashguards on the battery vent plug and inside the double lid are generally utilized to reduce the electrolyte loss, in the form of electrolyte droplets, during lifetime of maintenance-free batteries. Gas flow inside the battery cell and double lid is initially solved by finite volume method (FVM); then discrete phase model, in a Lagrangian reference frame, is employed to trace the electrolyte particles formed by bursting gas bubbles on the electrolyte surface and electrolyte splashing and agitating. In addition, appropriate physical models for the boundary conditions of the released gases, electrolyte droplets interaction with the lid walls and the flame arrestor are considered.

© 2008 Elsevier B.V. All rights reserved.

1. Introduction

Battery lid designers generally use baffles and splashguards in the vent plug or the battery lid in order to prevent the spillage of the electrolyte droplets due to two mechanisms. The first one is through accidental vibrating, splashing and agitating electrolyte in automobile movements, particularly during accelerating, braking and hitting a speed bump [1–5]. The second mechanism is frequently referred to as pumping. The latter occurs when the gas evolved in the battery bubbles around the electrodes. When the bubbles reach the electrolyte surface, they burst and sprinkle electrolyte droplets into the air. These electrolyte droplets may be carried toward the exhaust passageway by the gas flow [1,2,6,7].

Furthermore, designers consider other functions for these baffles including recombination of gases, condensation of vapors and prevention of electrolyte spillage due to battery tilting. Among them, so far the authors have studied the battery tilting by multiphase (electrolyte and air) modeling and CFD methods to find a practical tool to predict battery lid performance before prototyping [8]. In the present research, another phenomenon affecting battery lid performance has been studied by a number of physical models to find effective methods for designing battery lids [9]. Discrete phase model is utilized to trace the electrolyte particles formed by bursting gas bubbles and electrolyte agitating. In addition, appropriate physical boundary conditions for the released gases and electrolyte droplets interaction with the lid walls have been considered. Fluent software (version 6.1.22) is used to accomplish the simulations.

2. Model description

2.1. Bubble bursting phenomenon

During charging process in the battery, hydrogen and oxygen are produced in the form of bubbles. These bubbles rise to and burst on the surface of the electrolyte to produce both film and jet drops (Fig. 1).

The film drops are generated when the bubble film collapses and then the jet drops are produced due to the jet rising from the collapsing bubble cavity. The film drops have a size distribution of less than 0.1 to over 10 μm in diameter [10,11]. The diameter of jet drops does not vary in size significantly, only a factor of two or three, and is about one-tenth of the bubble diameter [12]. The number of film drops increases with bubble size. Although there is no film drop

* Corresponding author. Tel.: +98 21 88020741; fax: +98 21 88020741.
E-mail addresses: evahid@ut.ac.ir (V. Esfahanian), hmahmoodi@ut.ac.ir (H.M. Darian), hamedbab@me.ut.ac.ir (H. Babazadeh), m.aghvami@me.ut.ac.ir (M. Aghvami), rpasandeh@ut.ac.ir (R. Pasandeh), ftorabi@ut.ac.ir (F. Torabi), ahamdi@clarkson.edu (G. Ahmadi).

0378-7753/$ – see front matter © 2008 Elsevier B.V. All rights reserved.
doi:10.1016/j.jpowsour.2008.09.105

Nomenclature

A	area (m^2)
C	drag coefficient
d	diameter (m)
F	force (N)
g	gravity ($m\,s^{-2}$)
Q	volumetric flux ($m^3\,s^{-1}$)
Re	Reynolds number
t	time (s)
u, v, V	velocity ($m\,s^{-1}$)
We	Weber number

Greek letters

θ,φ	angle
μ	dynamic viscosity (Pa s)
ρ	density ($kg\,m^{-3}$)
σ	surface tension ($N\,m^{-1}$)

Subscripts and superscripts

D	drag
l	liquid
n	normal
p	particle
x	x direction

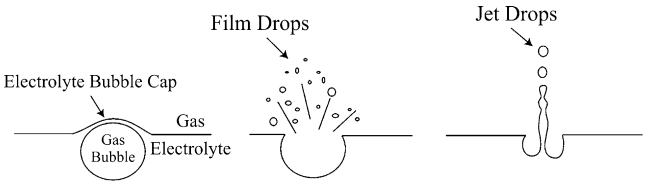

Fig. 1. Schematic representation of the burst of a bubble on the electrolyte surface.

production for 0.3-mm bubbles, a 6-mm bubble produces a maximum of 1000 film drops [12,13]. In contrast with film drops, the number of jet drops decreases with bubble size and never exceeds 10 [13]. Bubbles of less than 0.3 mm diameter produce five or more jet drops, whereas those of 6 mm produce only one [12]. Depending on their mass and initial velocity, these droplets will fall back into the electrolyte, flow out with the gas flow toward the vent or evaporate. When a jet is produced, the speed of the jet decreases as the size of the bursting bubble increases; for example, for 1 mm air bubbles bursting on water, a maximum jet speed of 6.4 ms^{-1} has been calculated and, for the rupture of 6 mm bubbles, the maximum jet speed reduces to 0.94 ms^{-1} (these speeds are for jets ejected into the atmosphere above the liquid [14]).

2.2. Droplet trajectory tracing

To predict the trajectory of a droplet, integration of the force balance on the particle written in a Lagrangian reference frame has been used. This force balance presents an equation between the particle inertia and the forces acting on the particle, which can be written (for the x direction), as

$$\frac{du_p}{dt} = F_D(u - u_p) + \frac{\rho_p - \rho}{\rho_p} g_x + F_x \tag{1}$$

where F_x is an additional acceleration (force per unit particle mass) term, $F_D\ (u - u_p)$ is the drag force per unit particle mass and $((\rho_p - \rho)/\rho_p)g_x$ represents the buoyancy force subjected to the droplets. The drag force is proportional to the droplet velocity relative to the stream velocity and its proportionality factor is defined as

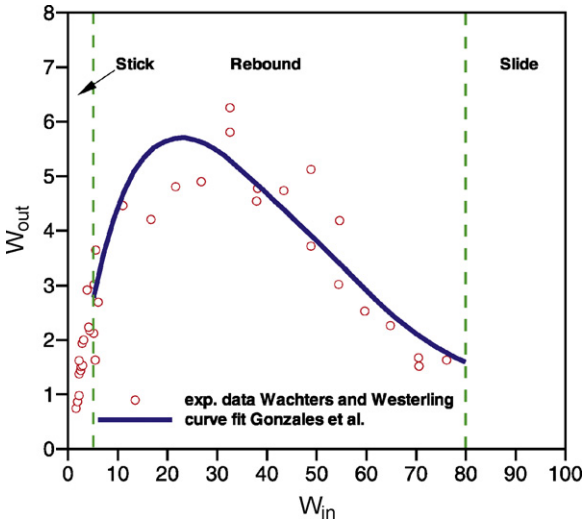

Fig. 2. Weber numbers of drops before and after strike.

$$F_D = \frac{18\mu}{\rho_p d_p^2} \frac{C_D\, Re}{24} \tag{2}$$

in which, u is the fluid phase velocity, u_p is the particle velocity, μ is the molecular viscosity of the fluid, ρ is the fluid density, ρ_p is the particle density, and d_p is the particle diameter. Re is the relative Reynolds number, which is defined as

$$Re = \frac{\rho d_p \left| u_p - u \right|}{\mu} \tag{3}$$

When a droplet reaches a physical boundary (e.g., a wall or inlet boundary) in the model, a discrete phase boundary condition will be applied to determine the fate of the trajectory at that boundary i.e. stick (trap), reflection (rebound), slide and so on. The most important parameter characterizing the impingement regimes is the Weber number:

$$We = \frac{\rho_l v_n^2 d}{\sigma} \tag{4}$$

which represents the ratio of the droplet's kinetic energy (v_n: velocity component normal to the surface, ρ_l: liquid density, d: droplet diameter) to its surface energy. The typical Weber number in this simulation is about 3. Based on Fig. 2 from Ref. [15], it can be concluded that the dominant phenomenon in this simulation is the stick of the droplets on the battery lid walls. In the stick regime, the droplets with low kinetic energy stick to the wall and they would not be followed further in this simulation.

3. Simulation description

In order to simplify the simulation and reduce its executing time, a single cell has been modeled instead of the whole battery (Figs. 3 and 4). Among different cells, the cell which is located next to the flame arrestor (and the vent of battery lid) has been selected because of its critical position (Fig. 3). Indeed, droplets can go out through this cell easier than other cells which are far from the vent of battery lid. Also in this cell, a zone between the free surface of the electrolyte (electrolyte–air interface) and flame arrestor is considered as the solution domain. Fig. 4 illustrates the different parts of the solution domain.

Fig. 3. Highlighted zone is used in the present simulation as the solution domain.

As shown in Fig. 5, about 300,000 computational cells are generated for this geometry using unstructured grid. The mesh is generated using Gambit software (version 2.2.30). The inlet of the simulation consists of two sources (Fig. 4). The First source is the continuous phase (hydrogen and oxygen gases) which is produced due to charge (and overcharge) reactions. To consider the most critical situation, overcharge reactions are used at the highest temperature of the battery (50 °C). According to Ref. [16] the total gas evolution (hydrogen and oxygen) for 1 A at 50 °C is 0.7420 $dm^3\,h^{-1}$. By considering 20 A in the most critical case for a starter lead-acid battery, the flow rate of continuous phase becomes 14.841 $dm^3\,h^{-1}$ resulting into a gas velocity of: $V_{gas} = Q_{cell}/A_{cell} = 5.58 \times 10^{-4}\ ms^{-1}$. This velocity has been used for the inlet of the continuous phase at the interface of the electrolyte and the air in the cell.

The second inlet source at the electrolyte–air interface is discrete phase droplets. As mentioned earlier, the droplets are produced through different phenomena. To consider all of these phenomena, a random distribution of diameter, velocity vector and injection position of these droplets has been applied in the range defined based on the source of the droplets. By increasing the number of droplets (random number), it is expected that the random distribution can properly model these phenomena inside the battery at unsteady conditions. The diameter range is selected from 10^{-5} m to 10^{-4} m, the magnitude of velocity is between 5 ms^{-1} and 7 ms^{-1}

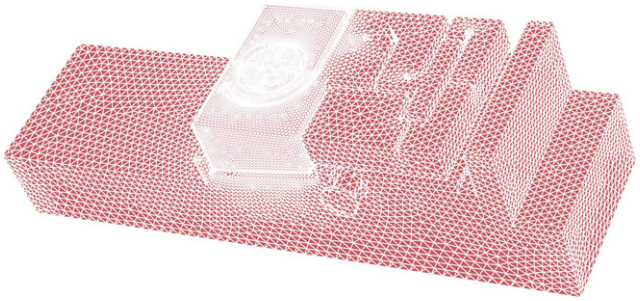

Fig. 5. Solution domain, three-dimensional mesh (about 300,000 computational cells) generated using unstructured grid.

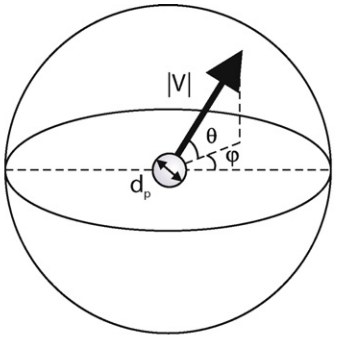

$1e\text{-}5 < d_p < 1e\text{-}4 \qquad 60^o < \theta < 90^o$

$5 < |V| < 7 \qquad 0^o < \varphi < 180^o$

Fig. 6. Typical range for the physical parameters of the injected droplets.

and its direction is limited to a cone (Fig. 6) between 60° and the right angle [17].

4. Results and discussion

In this simulation, a double lid without vent plug is used to investigate the battery lid performance. Fig. 7 shows the flow stream of the continuous phase (hydrogen and oxygen gases) which interacts with the discrete phase (electrolyte droplets). Although the lid does

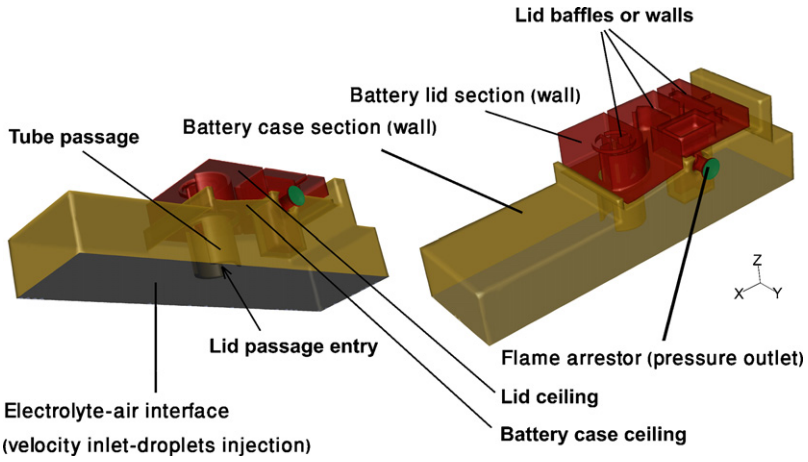

Fig. 4. Boundary conditions (mentioned in the parenthesis) of the battery model. Gray part: electrolyte–air interface as the gas inlet and also droplets injection face, green part: flame arrestor as the gas outlet, yellow part: battery case section as a wall, and red part: lid section as a wall. (For interpretation of the references to color in this figure legend, the reader is referred to the web version of the article.)

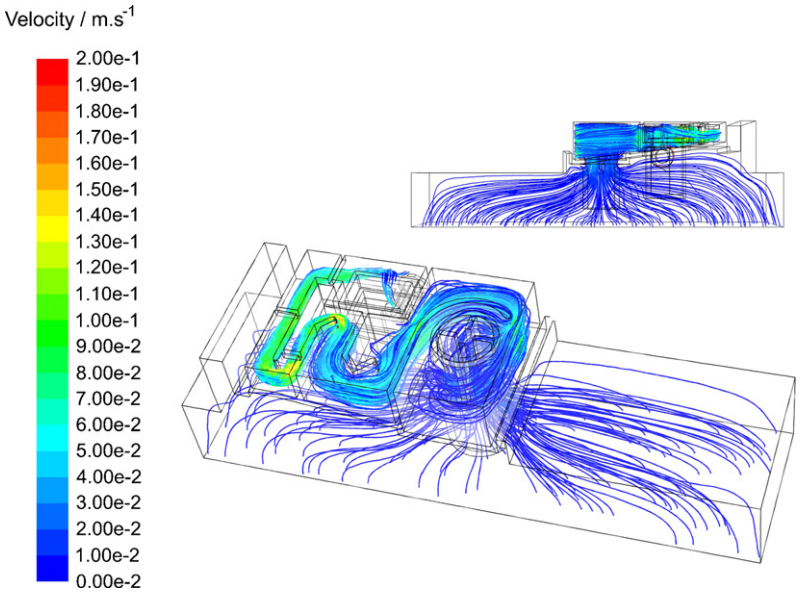

Fig. 7. Pathlines colored by velocity magnitude (ms^{-1}). Gas escapes from the battery through the flame arrestor.

not have any vent plug, some baffles are used at the top of the tube passage in order to prevent the droplets going upward.

As shown in Fig. 8, the injection distribution is random at the electrolyte–air interface to model all forms of droplet injection through different mentioned phenomena. These particles interact with continuous phase in each time step.

As shown in Figs. 8 and 9 few percent of all injected droplets can enter the lid passage and be trapped there. Tracing results show just 1.3 percent of the droplets, which are trapped or escaped, stick to the walls of the lid section. Seventy percent of the droplets are trapped on the battery case section ceiling and walls (Fig. 4) and the rest fall back into the electrolyte. Besides, Fig. 8 shows these droplets are trapped on the first rounded wall of the lid and its ceiling (Fig. 4). These trapped droplets can form bigger electrolyte drops which should be returned to the cell. To achieve such a criteria, the lid and baffles configuration should facilitate the electrolyte return. Therefore, using extra baffles as splashguards against exiting flow stream does not seem to be necessary. However, it should be noted that there are other functions for these baffles, i.e. condensation, recombination and returning the condensed or trapped droplets, which can be an area for future researches.

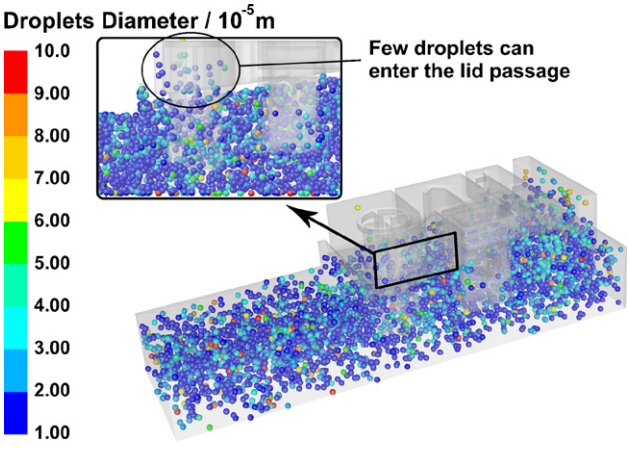

Fig. 8. Particle traces colored by particle diameter (m). Few percent of the droplets can enter the lid passage.

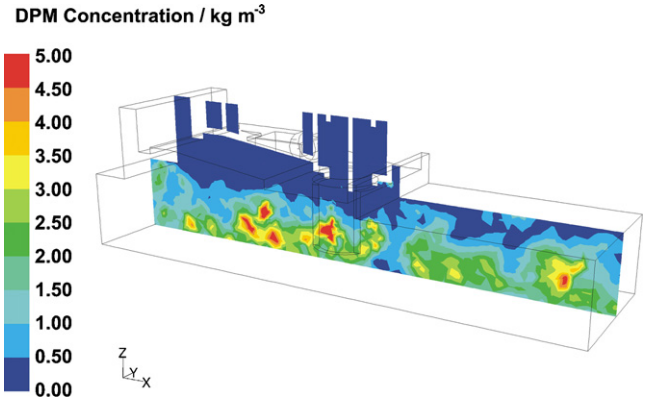

Fig. 9. Contours of discrete phase concentration ($kg\,m^{-3}$). Discrete phase concentration in the lid passage is very low.

5. Conclusions

In this paper, one of the important items in the battery lid design is studied by computational fluid dynamics (CFD). Electrolyte loss in the battery in the form of droplets can be reduced by using double lid especially for maintenance-free batteries. As shown in the present study, it is not necessary to use an extra number of complicated baffles and splashguards in the double lid or vent plug in order to prevent the electrolyte loss in the form of droplets. That is because almost all the droplets return back before entering the lid passage. This simulation can help the designer to study several items including lid walls configuration which are necessary to be considered in design of a battery lid before prototyping. It is important to note that other items such as battery tilting and condensation should be considered in designing the baffles and splashguards inside the double lid of maintenance-free batteries.

Acknowledgments

The authors wish to gratefully acknowledge the financial support from Niru Battery Manufacturing Co. and Vehicle, Fuel and Environment Research Institute of the University of Tehran.

References

[1] B.J. Thomas, W.J. Ross, Electrolyte baffling plug, United States Patent No. 6,277,517 (2001).
[2] B.J. Thomas, G.D. Slayton, J.R. Heinman, R. Barnett, electrolyte venting system with tubular splash guards, United States Patent No. 5,702,841 (1997).
[3] J.S. Leeson, J.F. Szabo, Vent plug system for batteries, United States Patent No. 4,072,799 (1978).
[4] D.T. Poe, Leak proof venting system for electric storage battery, United States Patent No. 5,691,076 (1997).
[5] W.R. Elehew, P.T. Kong, Anti-spill device for electrolyte battery, United States Patent No. 4,348,466 (1982).
[6] M.J. Shestok, G.D. Hudack, S.J. Cronrath, Storage battery gang vent cap, United States Patent No. 4,778,735 (1988).
[7] D.A. Thuerk, D.L. Smith, T.J. Dougherty, R.K. Hulsebus, Vent cap with electrolyte drain and explosion attenuation capabilities, United States Patent No. 5,284,720 (1994).
[8] V. Esfahanian, H. Mahmoodi, H. Babazadeh, H. Bahrami, H. Abedinpour, M. Aghvami, Numerical simulation of battery tilting test to investigate battery lid design characteristics, in: Proceeding of the 12th Asian Battery Conference, Shanghai, China, September, 2007.
[9] V. Esfahanian, H. Mahmoodi, H. Babazadeh, M. Aghvami, R. Pasandeh, H. Abedinpour, Numerical simulation of electrolyte particles trajectory to investigate battery cover design characteristics, in: Proceeding of the 7th International Conference on Lead-Acid Batteries LABAT'2008 Conference, Varna, Bulgaria, June, 2007, pp. 83–86.
[10] D.C. Blanchard, The Electrification of the atmosphere by particles from bubbles in the sea, Prog. Oceanogr. 1 (1963) 71–202.
[11] R.J. Cipriano, D.C. Blanchard, Bubble and aerosol spectra produced by a laboratory "breaking wave", J. Geophys. Res. 86 (C9) (1981) 8085–8092.
[12] D.C. Blanchard, L.D. Syzdek, Water-to-air transfer enrichment of bacteria in drops from bursting bubbles, Appl. Environ. Microbiol. 43 (5) (1982) 1001–1005.
[13] A.G. Guézennec, J.C. Huber, F. Patisson, Ph. Sessiecq, J.P. Birat, D. Ablitzer, Dust formation by bubble-burst phenomenon at the surface of a liquid steel bath, ISIJ Int. 44 (8) (2004) 1328–1333.
[14] J.M. Boulton-Stone, J.R. Blake, Gas bubbles bursting at a free surface, J. Fluid Mech. 254 (1993) 466–473.
[15] C. Baumgarten, Mixture Formation in Internal Combustion Engines, Springer–Verlag, 2006, p. 184.
[16] D. Berndt, Maintenance-Free Battery, 2nd ed., John Wiley & Sons Inc., Research Studies Press Ltd., 1997, p. 49.
[17] N.M. Aybers, A.K. Dagsoz, The mechanism of drop formation from gas or vapour bubbles, Warrme- and Stofftibertragung 1 (1968) 80–86.